Sedimentary evolution of the Le Danois contourite drift systems (southern Bay of Biscay, NE Atlantic): a reconstruction of the Atlantic Mediterranean Water circulation since the Pliocene

Shan Liu[a,b,c,*] shanliuu@hotmail.com, F. Javier Hernández-Molina[d], Gemma Ercilla[e], David Van Rooij[a]

[a]Department of Geology, Ghent University, Campus Sterre (building S8), Krijgslaan 281, B-9000 Gent, Belgium

[b]School of Marine Science, Sun Yat-sen University, Zhuhai, 519000, China

[c]Southern Marine Science and Engineering Guangdong Laboratory (Zhuhai), Zhuhai, 519000, China

[d]Department of Earth Sciences, Royal Holloway University of London, Egham, Surrey TW20 0EX, UK

[e]Institut de Ciències del Mar, CSIC. Continental Margins Group-GMC. Passeig Marítim de la Barceloneta 37-49, 08003, Barcelona, Spain

[*]Corresponding author at: Department of Geology, Ghent University, Campus Sterre (building S8), Krijgslaan 281, B-9000 Gent, Belgium.

Abstract

The evolution of the Le Danois contourite depositional systems (CDS) during the Pliocene and Quaternary was investigated based on high-resolution seismic reflection data. From old to young, six seismic units (U1 to U6) bounded by major discontinuities (H1 to H6) were identified. Regarding variations of the bottom-current circulation, four evolution stages of the Le Danois CDS were identified, including onset (~5.3 to 3.5-3.0 Ma), initial (3.5-3.0 to 2.5-2.1 Ma), intermediate (2.5-2.1 to 0.9-0.7 Ma) and drift-growth (0.9-0.7 Ma to present day) stages. The CDS associated with the Atlantic Mediterranean Water (AMW) along the middle continental slope initiated at ~3.5-3 Ma and was widely built after the Mid-Pleistocene Transition (MPT; 0.9-07 Ma). At a shallower water depth, a second CDS associated with the Eastern North Atlantic Central Water (ENACW) started to develop from the late Quaternary (~0.47 Ma) onwards. In the AMW-related drift system, the Le Danois Drift was generated both under glacial and interglacial climatic oscilations. Repeated internal structures in unit 5 that consist of acoustically transparent lower parts, moderate amplitude upper parts and high amplitude erosional surfaces at the top, are compared with interglacial/glacial cycles since the middle Pleistocene to the present day. These cyclic features suggest coarsening-upward sequences of the Le Danois Drift and processes related to enhanced AMW during glacial stages. The estimated sedimentation rate of the Le Danois CDS reached a maximum during the MPT (at least ~27 cm/ky) and then decreased until present-day (~5 cm/ky). Variations of sedimentary stacking patterns and processes of the Le Danois CDS imply full domination of the intermediate water mass along the central Atlantic and southwest European continental slopes from the late Pliocene (~3.5-3.0 Ma) onwards.

Keywords: seismic stratigraphy; contourite depositional system; bottom currents; continental margin evolution; southern Bay of Biscay

1 Introduction

Contourite drifts are extensive sediment bodies built up through the action of alongslope bottom currents (Rebesco et al., 2008). When contour-following alongslope processes dominate over gravitational downslope processes along continental margins, Contourite Depositional Systems (CDS) may develop as various depositional (drifts) and erosive features (Hernández-Molina et al., 2008). In the NE Atlantic, circulation of the Mediterranean Outflow Water (MOW) leads to the generation of persistent bottom currents along the southwest European continental margin (van Aken, 2000b; Rogerson et al., 2012). In order to be able to distinguish pure thermohaline outflow (MOW) in the most proximal site to the source (the Strait of Gibraltar at the Gulf of Cádiz), the modified waters in the NE Atlantic are referred to as the Atlantic Mediterranean Water (AMW) (Rogerson et al., 2012; Fletcher et al., 2015; Liu et al., 2019). Domination of Mediterranean water along the North Atlantic margins has resulted in the development of various contourite drifts and CDS (Collart et al., 2018; Hernández-Molina et al., 2011; Llave et al., 2006; Mena et al., 2018; Van Rooij et al., 2010, 2007; Liu et al., 2019). These contourites display large variations in size, shape and vertical position along MOW/AMW pathways, thus provide valuable sedimentary records of the margin evolution and paleoceanography (Van Rooij et al., 2007; Ercilla et al., 2011; García et al., 2016; Hernández-Molina et al., 2016).

In the Gulf of Cádiz, the generation of the Cádiz CDS coincided with the first MOW enhanced stage during the early Pliocene (Llave et al., 2011; Roque et al., 2012; van der Schee et al., 2016). From the early Quaternary (~2 Ma) onwards, the Cádiz CDS experienced a major growth stage (Hernández-Molina et al., 2016). At the distal AMW site, sediment records from Goban Spur and Porcupine Seabight document extreme erosive events resulted from the AMW since the late Pliocene (Van Rooij et al., 2007; Huvenne et al., 2009; Thierens et al., 2013; Delivet et al., 2016). The ages of erosional events are difficult to reconstruct from sediment thicknesses and stacking pattern data due to erosional activities (Raddatz et al., 2011). Fast accumulation rates of the Porcupine CDS have only been recorded after the middle Pleistocene (0.725–0.65 Ma), which is more than ~1 My late compared to the Cádiz CDS (Huvenne et al., 2009; Hebbeln et al., 2016). There are still temporal gaps of MOW/AMW variability from proximal to distal sites. As such, a linkage between the Gulf of Cádiz and Porcupine Seabight is needed to document regional paleocirculation and associated sedimentary influences along the continental margins.

The Cantabrian continental margin (Fig. 1), positioned between the Gulf of Cádiz and Porcupine Seabight, lies in an understudied region with regard to AMW paleoceanography. Extensive submarine canyon systems interrupted alongslope transport of sediments, suggesting that downslope processes dominated (Weaver et al., 2000; Toucanne et al., 2008; Mulder et al., 2012). However, contourite depositional systems are identifiable among these canyon systems (Ercilla et al., 2008; Iglesias, 2009; Van Rooij et al., 2010; Liu et al., 2019), providing a unique opportunity to exam the AMW paleoceanography at an intermediate site. In the Le Danois Bank region, there are three water masses; 1) Eastern North Atlantic Central Water (ENACW), 2) AMW and 3) Labrador Sea Water (LSW) (Liu et al., 2019). Topographically constrained morphologies strongly intensify bottom currents, resulting in more frequent spatial variations of the related contourite features (González-Pola et al., 2012; Liu et al., 2019). A regional seismic stratigraphy of the Le Danois CDS has been addressed by Van Rooij et al. (2010), albeit on a relatively small set of seismic profiles. The CDS initiated during the early Pliocene and underwent a major growth stage from the late Pliocene onwards (Van Rooij et al., 2010). However, detailed insight of Pliocene-Quaternary sedimentary processes and evolution of the Le Danois CDS, as well as past circulation patterns of the AMW, are not well understood.

This work describes the seismic stratigraphy and sedimentary stacking patterns of the Le Danois CDS. The main objectives of this study are: (1) to document the temporal variability of contourite features; (2) to discuss sedimentary processes and evolution of drift systems; (3) to improve the understanding of past dynamics of intermediate water masses through the late Pliocene to the present day along the Cantabrian continental slope. The location of the Le Danois CDS is key for understanding past AMW variability between its proximal and distal sites. Newly acquired seismic data allows the identification of Le Danois contourite features in a higher lateral and temporal resolution.

2 Regional setting

2.1 Geological setting

The Le Danois Bank region, located at the Cantabrian continental margin, consists of an intraslope basin, the Le Danois Bank, the Lastres Canyon and the Asturias continental shelf (Figs. 1a, 2c). Contourite drifts and associated moats are present in the intraslope basin (Van Rooij et al., 2010; Liu et al., 2019). Among them, the Le Danois Drift is located between 790 and 1080 m water depth, while the Gijón Drift is located between 320 m and 1060 m water depth (Fig. 2c). The small Asturias Drift covers an area of 21 km^2 at

water depths between 900 and 1080 m. Besides these elongated and mounded drifts, six plastered drifts are recognized along the southern flank of the Le Danois Bank and at the upper continental slope (Liu et al., 2019).

The Le Danois Bank originated from the Iberian rifting and extensional events during the Late Permian (Ries, 1978; Costa and Rey, 1995; Catalán et al., 2007). During the Triassic and Jurassic, extension continued with extreme crustal thinning in the Bay of Biscay. (Tugend et al., 2014). During the Cretaceous, northward displacement of the African Plate changed plate kinematics and led to an uplift of the Cantabrian Mountains (Gallastegui et al., 2002). After a tectonically stable stage in the Paleocene, the Le Danois Bank and the intraslope basin started to deform due to shortening of the Northern Iberian margin during the Eocene (Alvarez-Marrón et al., 1996; Cadenas and Fernández-Viejo, 2017). During the Oligocene, crustal shortening of the former continental slope resulted in E-W orientated faults within the intraslope basin (Boillot et al., 1979; Gallastegui et al., 2002; Vissers and Meijer, 2012). From the late Eocene to early Miocene, tectonic inversion of extensional Mesozoic faults occurred (Zamora et al., 2017). No major deformation or tectonic activities are observed since the early Miocene (Fig. 1b) (Cadenas and Fernandez-Viejo, 2016; Zamora et al., 2017).

2.2 Present-day oceanography

Present-day circulation pattern within the Le Danois Bank region is dominated by the ENACW, the AMW and the LSW (Fig. 1a). ENACW mainly penetrates eastwards along the Asturias continental slope between 350 to 600 m and forms an anticyclonic circulation along the rim of the eastern summit of the bank (González-Pola et al. 2012). The core of this water mass is centred at 400 m with a minimum salinity of about 35.5 (van Aken, 2000b; Lavín et al., 2006). Below the ENACW and the mixing layer, the warm (9°-10.5° C) and saline (35.7-35.9) AMW flows between 750 to 1550 m, while its core is positioned at 1000 m (Iorga and Lozier, 1999; van Aken, 2000b; Lavín et al., 2006). The AMW mainly penetrates eastwards along the outer (northern) flank of the Le Danois Bank (Lavín et al., 2006; González-Pola et al., 2012; Liu et al., 2019). Along the southern flank of the bank, a branch of the AMW flows in a westward direction (González-Pola et al., 2012). Between 1750 and 2000 m water depth, LSW penetrates westwards below AMW and the mixing layer (van Aken, 2000a). The core is recognized at 1800 m with a salinity minimum at about 35.05 (Pingree and Le Cann, 1990; van Aken, 2000a). It mainly follows the outer flank of the Le Danois Bank (Lavín et al., 2006). Along the southern base of the bank, a branch of LSW flows westwards to the intraslope basin. Compared to background flow velocities (1-5 cm/s; Iorga and Lozier, 1999), bottom

currents from these three water masses are strongly enhanced (estimated acceleration up to 25 cm/s) due to the topographic control of the Le Danois Bank (Liu et al., 2019).

2.3 AMW paleoceanography

Before the establishment of the present-day oceanographic conditions, the past ENACW, AMW and LSW varied in physical structure, circulation regime and flowing depth (Hillaire-Marcel et al., 2001; Voelker et al., 2006; Rogerson et al., 2010; Bahr et al., 2015). At the latest Miocene/early Pliocene (< 5.33 Ma), the initiation of the present-day Atlantic-Mediterranean exchange resulted in the formation of MOW (Hernández-Molina et al., 2014; van der Schee et al., 2016). At ~4.5 Ma, MOW circulated into the Gulf of Cádiz (Hernández-Molina et al., 2014) which resulted in the stratification of ENACW and MOW/AMW (Jia et al., 2007; Volkov and Fu, 2010). During the late Pliocene (3.2-3.0 Ma) and early Quaternary (2.4-2.0 Ma), MOW had an enhanced circulation regime and extended poleward (Hayward et al., 2009; Raddatz et al., 2011; Khélifi et al., 2014). At ~1.8 Ma, LSW was stratified from the North Atlantic Deep Water (NADW) and flowed below the MOW/AMW (Burton et al., 1997). By this time, pathways of these water masses started to resemble their modern pathways (Raymo et al., 2004; Rogerson et al., 2012).

During the Mid-Pleistocene Transition (MPT, ~1.25-0.7 Ma), the periodicity of Earth's climate cycles dramatically changed from 41 ky to 100 ky (Maslin and Ridgwell, 2005; Elderfield et al., 2012). As a result, glacial/interglacial fluctuations started to significantly influence the properties and dynamics of these water masses (Llave et al., 2006; Expedition et al., 2007; Kaboth et al., 2016; Bahr et al., 2018). The MOW/AMW was 300-700 m deeper and bottom currents were more vigorous during glacial periods (Rogerson et al., 2005; Voelker et al., 2006; Kaboth et al., 2016). During interglacial periods, AMW was weaker and located between 600 and 1000 m water depths (Schönfeld and Zahn, 2000; Rogerson et al., 2005). Increased MOW production promoted the ENACW, in turn resulting in strong ENACW currents (Bahr et al., 2018).

During the middle Pleistocene (~420-396 ka), the ENACW was continuously enhanced during glacial intervals due to domination of the Iberian Poleward Current (IPC) (Voelker et al., 2015). However, MOW/AMW was largely unaffected by glacial-interglacial cycles between ~0.47 Ma and ~0.13 Ma (Kaboth et al., 2017). LSW was unstable during climate cycles due to the reduced production of the NADW (Hillaire-Marcel and Bilodeau, 2000). During the Last Glacial Maximum (LGM), ENACW extended northwards to the Bay of Biscay (Bender et al., 2012; Mena et al., 2018). Below ENACW, the core of AMW prevailed at a deeper depth (2000 m) due to increased density (Schönfeld and Zahn, 2000). Between 7.5

and 6 ka, the core of AMW retreated to 1000 m (Schönfeld and Zahn, 2000). Finally, the modern circulation of ENACW, MOW/AMW and LSW was established at ~15.5 ka, ~7.5-6 ka and ~7 ka, respectively (Schönfeld and Zahn, 2000; Hillaire-Marcel et al., 2001; Bender et al., 2012; Mena et al., 2018).

3 Methodology

This study is based on single channel sparker and multi-channel airgun reflection seismic data (Fig. 2a). High-resolution single channel seismic data were acquired using a 500 J energy SIG sparker (120 electrodes) during the R/V Belgica cruise ST1118a in 2011. Penetration of the acoustic signal is around 500 ms TWT. The dominant frequency is around 800 Hz and vertical resolution is about 1.5 m. A total of 27 sparker seismic lines, with a NNE-SSW (12 lines) and W-E to WNW-ESE (15 lines) orientation and with a 3-5 km spacing were acquired (Fig. 2a). Multi-channel airgun seismic data was obtained by a 150 m SIG streamer during the BIO HESPERIDES campaign MARCONI II in 2003. Penetration depth of the acoustic signal varies around 1.5 s TWT. The dominant frequency is around 80 Hz and the vertical resolution is about 4.5 m. A total of 26 airgun seismic lines were acquired with NNE-SSW (17 lines) and WNW-ESE (9 lines) orientations and a 10-15 km line spacing (Fig. 2a).

Seismic data processing was performed using Delph Seismic Plus and the DECO Geophysical RadexPro software. The sparker seismic data was processed using a swell filter and an Ormsby bandpass filter (160–250 Hz and 1400–1500 Hz). A bandpass filter (2.5 kHz high pass and 80 kHz low pass), a spherical divergence correction, an interactive velocity analysis and a burst noise removal were applied for processing of the airgun seismic data. Seismic interpretation was carried out in the IHS Kingdom Suite™ package. Seismic reflection travel time between each horizon and the seafloor was gridded to produce isopach maps. A minimum curvature is used as gridding method to avoid sharp boundaries of sediment bodies that might result from spacing (3-15 km) of the seismic profiles. Depths were converted from seconds two-way-travel time to metres by using a velocity model (Fig. 2b) derived from published borehole data (Cadenas and Fernandez-Viejo, 2017). The calculation of sedimentation rates is based on a time to depth conversion of each horizon, tied to their estimated chronostratigraphy.

The stratigraphic divisions for major depositional units was based on the identification of regional unconformities (Fig. 3). Two additional criteria were used for the recognition of subunits. The first uses the vertical variation of acoustic facies, which was applied to separate subunits of units 3 and 4. The other criterion uses local erosional discontinuities, which was used to identify subunits of units 5 and 6.

4 Results

4.1 Seismic stratigraphic framework

Based on seismic interpretation of the sparker and airgun seismic profiles, six seismic units (U1 to U6) bounded by major discontinuities (H1 to H6) have been identified from old to young, respectively (Fig. 3, Table 1). The penetration of the sparker source (~500 ms TWT, while ~1500 ms TWT for airgun source) inhibits observation of the lowermost unit 1 (Figs. 4, 5). Unit 2 can only be recognized within the northern part of the intraslope basin (Figs. 3, 4), whereas both units could be identified in airgun seismic profiles (Figs. 6a, 7, 8, 9). Below unit 1, several buried structural highs are observed, characterized by medium-high amplitude chaotic and discontinuous reflections (Fig. 7). Seismic features within subunits are hard to be observe in the airgun seismic data due to the reduced vertical resolution (4.5 m) with respect to sparker seismic profiles (vertical resolution of about 1.5 m). At some locations, where seismic reflections thin and show pinch-out, the subunit boundaries are uncertain and are identified in tracing continuous high amplitude reflections.

4.1.1 Unit 1

Unit 1 is bound by H1 at base. H1 is an unconformity with strong high-amplitude reflections (Fig. 8). Onlap terminations are observed onto the basement (H1) while toplap terminations towards the top are recognized (Fig. 7). The seismic facies of unit 1 consists of low-moderate amplitude, semi-continuous transparent-subparallel reflections (Fig. 7). This unit is mainly observed in the mini-basins between buried structural highs. The thickness of unit 1 ranges from 250 ms to 350 ms TWT at the intraslope basin centre (Fig. 8). Towards the Le Danois Bank and the continental shelf, its thickness gradually declines to 20-80 ms TWT.

The depth and the width of the mini-basins vary between 50 to 350 ms TWT and 3.5 to 12.5 km, respectively. Most of these mini-basins are located along the northern and southern boundaries of the Le Danois intraslope basin (Fig. 7). The largest mini-basin is positioned at the central part of the intraslope basin (Fig. 5). Additionally, various buried structural highs are located along the southern and northern boundaries of the intraslope basin (Figs. 4, 5, 6, 9). They have an average length of 10-20 km and a width of 5-6 km (Fig. 7).

4.1.2 Unit 2

Unit 2, characterized by high amplitude, disrupted/semi-continuous chaotic-subparallel reflections, is separated from unit 1 by reflection horizon H2 (Figs. 4, 8). At its base, unit 2 displays onlap terminations towards the Le Danois Bank and buried structural highs (Fig. 6c), whereas onlap and downlap terminations are shown at the central part of the intraslope basin (Fig. 6a). Towards the top of unit 2, toplap and truncations are recognized (Figs. 5, 7). This unit is mainly distributed within the mini-basins (Figs. 6c, 7). At the southern and northern parts of the intraslope basin, unit 2 overlies two buried structural highs (Figs. 6a, 9). Its thickness reaches a maximum of 310 ms TWT at the centre of the Le Danois intraslope basin (Fig. 6a). Towards the Le Danois Bank, unit 2 gradually thins with a thickness reduction to 10 ms TWT (Fig. 8).

4.1.3 Unit 3

Unit 3 is bound by H3 at its base. H3 is an erosional unconformity with high amplitude reflections (Figs. 4, 8). Onlap and downlap terminations are observed onto H3, while toplap and truncations towards the top of the unit are recognized. Mounded features are only identified at the base of the northern side of the intraslope basin, with a thickness of about 200 ms TWT and a width of 5 km (Fig. 7). Elsewhere in the intraslope basin, this unit mainly fills the mini-basins with subparallel reflections from the centres and divergent reflections towards buried structural highs (Fig. 4). At the top of a buried structural high, which is located within the central part of the northern boundary of the Le Danois intraslope basin, continuous subparallel reflections are partly disrupted by fault-like features (Fig. 4).

Unit 3 consists of two subunits, 3a and 3b, from bottom to top. They are separated by a conformable boundary represented by a high amplitude reflection (Fig. 4). Unit 3a is characterized by low-moderate amplitude, continuous subparallel-oblique reflections (Figs. 4, 6c). The thickness is about 70 ms TWT and decreases towards the buried structural highs and the Le Danois Bank. Compared with unit 3a, unit 3b has similar reflections, but higher (moderate-high) amplitude and greater thickness (90-110 ms TWT) (Fig. 4). At the top of unit 3b, erosional features with truncated reflections are present at the northeast boundary of the intraslope basin (Figs. 6, 8).

4.1.4 Unit 4

Unit 4 is bound by H4 at its base and consists of moderate-high amplitude and continuous oblique-subparallel reflections (Figs. 4, 8). Low-angle downlap and onlap are recognized onto H4, while high-angle truncated terminations are widely observed at the top of unit 4. Some parts of unit 4 are eroded in the

intraslope basin (Figs. 5, 7). The associated erosional surfaces are distributed along the southern base of the Le Danois Bank and the uppermost continental slope, where the extent of erosion is about 5-7.5 km wide, 68 km long and 7.5-10 km wide, 27 km long, respectively (Fig. 10d). The thickness of the unit varies and, because of extensive erosion, its preservation is poor. The least eroded part, positioned at the centre of the basin, is 20-100 ms TWT thick. Internal structures of unit 4 display moderate-high amplitude, semi-continuous wavy reflections (Fig. 4). Their wavelength is about 1.5-2 km and the wave height about 10-20 ms TWT. Along the easternmost boundary of the intraslope basin, low-moderate amplitude, continuous subparallel reflections and an elongated geometry were observed in unit 4 (Figs. 7, 9). Its thickness is greater (varies from 100-240 ms TWT) compared to the wavy section at the basin centre.

On the basis of seismic facies and reflection terminations, three subunits, being units 4a, 4b and 4c, are discerned from the bottom to the top of unit 4 (Fig. 4). These subunits are distributed at the central part of the Le Danois intraslope basin. Unit 4a has a relatively greater thickness compared with units 4b and 4c (Figs. 4, 5). In unit 4b, wavy features are better developed and show moderate amplitude at the centre of the intraslope basin (Fig. 4). Unit 4c, characterized by high amplitude reflections, are widely eroded and is only present at the basin centre (Figs. 4, 5). The average thickness of these subunits is about 30 ms TWT.

4.1.5 Unit 5

H5, marked as the base of unit 5, is the most prominent erosional unconformity of the entire seismic sequence (Figs. 4, 8, 9). Low-angle onlap and downlap are observed onto H5, while low-angle toplap terminations are recognized at the top of unit 5. Along the southeast base of the Le Danois Bank (Fig. 8) and the southern flank of a structural high (Fig. 6c), Le Danois and Asturias drifts shows mounded features with an upslope progradation within this unit. The thickness is 100-150 ms TWT and laterally thins towards the west. Whereas along the southwest boundary of the intraslope basin, the thickness is 120-200 ms TWT and laterally decreases towards the east. Three moat features are observed associated with a mounded geometry at these locations. They are 1-2 km wide and 10-50 ms TWT deep. Along the southeast boundary of the intraslope basin, reflections laterally change from subparallel to chaotic. Towards the centre of the basin, sigmoidal and mounded features diminish in size. The thickness of unit 5 declines towards the E-W trending axis of the intraslope basin and partly drop to 5 ms TWT (Fig. 4).

Four subunits (units 5a, 5b, 5c, 5d) are present in unit 5 from the bottom to the top. These subunits consist of an acoustically transparent lower part, a moderate amplitude upper part and a high amplitude

erosional surface at the top (Figs. 3, 4). The average thickness of unit 5a is 40 ms TWT. From units 5b towards 5d, the thickness reduces from 50 to 10 ms TWT.

4.1.6 Unit 6

Unit 6 is bounded by H6 at base and the seafloor at top. H6 is an unconformity and has high-amplitude reflections. Toplap terminations towards the seafloor, onlap and downlap terminations onto H6 are observed in unit 6. Along the entire southern base of the Le Danois Bank (Fig. 8) and the southern flank of a structural high (Fig. 6c), mounded features are observed in unit 6. The thickness at these locations is around 50-100 ms TWT. Mounded geometries are identified along the entire southern boundary of the intraslope basin as well (Figs. 5, 7), where the thickness is measured as 100-150 ms TWT. Three moat features associated with the mounded seismic sequence could be identified at these locations. They are around 1-2 km in width and 10-40 ms TWT in depth. Along the eastern boundary of the intraslope basin, the internal structure of unit 6 is characterized by acoustically transparent-subparallel interbedded reflections (Fig. 7). These interbedded features extend towards the east and the unit thickness gradually declines from 150-190 to 50 ms TWT. Along the upper continental slope, the southern flank and the southeast base of the Le Danois Bank, plastered seismic sequence with a thickness of 10 ms TWT are identifiable. Unit 6 consists of four subunits: units 6a, 6b, 6c, and 6d from bottom to top, respectively. The thickness of these subunits is constant (20 m. TWT) and the amplitude of reflections has small variations (moderate-high amplitude) (Fig. 5).

4.2 Contourite depositional and erosional features

Le Danois Drift, encompassing an area of 242 km^2, has a mounded geometry with largely continuous parallel-stratified reflections and a sigmoidal pattern where it onlaps the structural high (Fig. 4). The mean thickness of this drift laterally decreases from 280 to 130 ms TWT towards the south (Figs. 7, 8). The sedimentary body of the Le Danois Drift consist of units 3, 5 and 6. The U-shaped profile of the associated Le Danois Moat starts to show from unit 3b (Fig. 6).

The Gijón Drift covers an area of 254 km^2. It has a broad mounded geometry and is composed of unit 5 and 6 (Fig. 5). The associated Gijón Moat has an asymmetric U-shape profile (Fig. 5). The Gijón Drift is characterized by stratified layers of continuous sigmoidal reflections interbedded with discontinuous low-amplitude chaotic reflections (Fig. 7). Its thickness gradually decreases from 320 to 30 ms TWT towards the southeast (Fig 7).

The Asturias Drift is smaller in size, which covers an area of 21 km^2. It displays a sigmoidal-oblique seismic stacking pattern and the maximum thickness is 90 ms TWT, decreasing towards the southwest (Fig.6). The drift overlies H5 and consists of units 5 and 6 (Fig. 6c).

5 Discussion

5.1 Chronostratigraphic framework

The chronostratigraphic framework in this study is established through the correlation of the seismic stratigraphy with limited regional borehole information (Cadenas and Fernandez-Viejo, 2017),. The tectonic and sedimentary evolution of the Cantabrian continental margin was described from seismic reflection data and borehole logs, which allowed the construction of a tentative chronostratigraphic framework (Ercilla et al., 2008; Iglesias 2009; Van Rooij et al., 2010; Cadenas and Fernandez-Viejo, 2016). Borehole MC H-1X, the only well located in the intraslope basin (Fig. 2a), only recovered sediments with a Cretaceous-Eocene age (Cadenas and Fernandez-Viejo, 2017). Only the Cretaceous and Eocene unconformities from this well were tied to current seismic data, based on a rudimentary depth to time conversion (Figure 5.a). Iglesias (2009) correlated this well with other boreholes that are located at the Asturias continental shelf. However, all these onshore and offshore boreholes only reached parts of sedimentary cover. Density or P-wave data and biostratigraphic information of sedimentary sections younger than the Miocene are not available (Iglesias, 2009; Cadenas and Fernandez-Viejo, 2017). The resolution of the borehole data did not allow the identification of a detailed chronostratigraphy from the Pliocene to the present day.

The Pliocene-Quaternary seismic section of the Le Danois intraslope basin mainly consists of erosional and depositional contourite features shaped by the AMW (Ercilla et al., 2008; Iglesias 2009). Seismic architectures associated with these features, as well as the occurrence of major unconformities, are linked with AMW variability since Pliocene times (Van Rooij et al., 2010). The seismic sections and imaged unconformities correlate between MOW/AMW related drifts because they were all affected by the same water mass. The Le Danois CDS shows similar seismic characteristics by comparing with those in the Gulf of Cádiz (Hernández-Molina et al., 2016) (Fig. 3), along the SW Portuguese margin (Teixeira et al., 2019), in the Landes Plateau (Faugères et al., 2002), in Goban Spur (Delivet et al., 2016) and Porcupine Seabight (Van Rooij et al., 2007). These regions are namely located along the pathways of the MOW/AMW from the proximal to distal sites (Hernández-Molina et al., 2011). As such, the Pliocene-Quaternary

chronostratigraphic framework of the Le Danois Bank region is tentatively correlated with established stratigraphic frameworks from these regions to mark major erosion events and/or changes in circulation patterns of the AMW (Fig. 3). However, the accuracy of the chronostratigraphy is uncertain in this study due to data limitations.

5.1.1 H1: Lower Miocene

Triassic to Quaternary seismic units were recognized in the area by Cadenas and Fernandez-Viejo (2017) by tying seismic reflection data to offshore well logs. Their study has correlated the well MC H-1X with other boreholes on the continental shelf, indicating a regional lower Miocene discontinuity, which is about 1.2 s TWT deep at the location of well within the intraslope basin (Cadenas and Fernandez-Viejo, 2017). This regional discontinuity from their study is tentatively correlated with horizon 1 from this study through connecting seismic profiles (Figs. 6a, b). As such, H1 could be considered as the late Miocene discontinuity.

5.1.2 H2: Upper Miocene

Ercilla et al. (2008) and Iglesias (2009) discussed the Oligocene-Quaternary seismic sequence of the Le Danois Bank region with a higher resolution than studies dealing with the tectonic evolution of the area (Gallastegui et al., 2002; Cadenas and Fernandez-Viejo, 2016). Horizon I from their studies is considered as a regional unconformity that separates the underlying low-moderate amplitude unit and the overlying high reflective seismic unit (Ercilla et al., 2008; Iglesias, 2009). This significant change in seismic facies is related to the occurrence of gravity flows and mass-movements at the end of the Miocene (Iglesias, 2009). A similar seismic feature is observed in units 1 and 2 of this study, suggesting similar time intervals (Fig. 3). Indeed, horizon I is correlated with H2 of this study (Fig. 9). Therefore, unit 1 is attributed a Miocene age and H2 is considered to be the top of the Miocene.

5.1.3 H3: Late Pliocene

In the intraslope basin, the formation of the Le Danois Drift initiated in unit 3, where the first seismic evidence of mounded features is observed. Previous studies demonstrate the linkage between Le Danois Drift and AMW (Van Rooij et al., 2010). Thus, unconformities resulted from MOW/AMW in other regions could correlate with those of Le Danois Drift. Acoustic responses (low to high amplitude from the base to the top) in Pliocene units of the Cádiz CDS (Llave et al., 2011; Roque et al., 2012; Hernández-Molina et al., 2016; Lofi et al., 2016; van der Schee et al., 2016) and the Sines contourite drift (Teixeira et al., 2019) compare with seismic facies of Le Danois Drift in unit 3. The basal unconformity, being the LPD (late

Pliocene discontinuity, 3.2-3.0 Ma; Hernández-Molina et al., 2016), marks the initiation of mounded contourite drift formation in the Cádiz CDS. Additionally, cold-water corals (CWC), fed by food particles transported by the AMW, and associated contourite drifts started to grow and develop upon the RD-1 unconformity in Porcupine CDS during the late Pliocene (Van Rooij et al., 2007; Huvenne et al., 2009). Evidence of AMW enhancement during the late Pliocene are linked with the onset of the Le Danois Drift deposition. As such, H3 is tentatively associated with the LPD (Fig. 3).

5.1.4 H4: Early Quaternary

The EQD (the early Quaternary discontinuity; at ~2.4-2.0 Ma) observed within the Cádiz CDS and Goban Spur is attributed to a second major MOW/AMW intensification phase of (Llave et al., 2007; Lofi et al., 2016). This stage coincides with the final enhancement of the northern hemisphere glaciation (NHG) during the early Quaternary (Friedrich et al., 2013; Hernández-Molina et al., 2014). Consequently, erosive features are observed along the entire NE Atlantic margins during this time interval (Faugères et al., 2002; Van Rooij et al., 2007; Roque et al., 2012). H4 is a major erosional unconformity in the Le Danois intraslope basin and can be compared with the EQD due to highly reflective seismic facies and associated reflection termination (Figs. 5, 8). Thus, H4 is considered to have an early Quaternary age. The Le Danois CDS is located at the intermediate site of the AMW. The possible age of H4 ranges between~2.5 Ma and ~2.1 Ma.

5.1.5 H5: Middle Pleistocene

In unit 5, contourite drifts with mounded features are widely generated in the intraslope basin. The basal unconformity is the most prominent erosional surface (Fig. 7) and compares with those of the Gulf of Cádiz and Porcupine Seabight (Van Rooij et al., 2007; Huvenne et al., 2009; Llave et al., 2011; Hernández-Molina et al., 2016). These erosional surfaces are presumed to have results from the winnowing of MOW/AMW and are considered to be the MPD (Mid-Pleistocene discontinuity; 0.9-0.7 Ma), associated with the Early-Middle Pleistocene Climate Transition (MPT) (Llave et al., 2011; Huvenne et al., 2009). Since the MPT, global climate cycles of long glaciations and short deglaciations significantly influenced the MOW/AMW regime in the NE Atlantic (Lisiecki and Raymo, 2005; Hernández-Molina et al., 2014). The related third major intensification of the MOW/AMW resulted in widely distributed erosional features, especially in areas adjacent to topographic obstacles and basement highs along the NE Atlantic margins (Van Rooij et al., 2007; Llave et al., 2011; Roque et al., 2012; Hernández-Molina et al., 2016). Similar erosional characteristics are observed in the Le Danois intraslope basin as well (Fig. 6). As such, H5 is

linked to the MPD. The accurate age of H5 is unknow due to the data limitation. Erosive processes that generated H5 should be coeval with the winnowing stage of MOW/AMW. The age of H5 most likely varies between 0.9 Ma and 0.7 Ma.

5.1.6 H6: Late Quaternary

H6 is the youngest major unconformity of this study. The latest major discontinuity is marked as the LQD (late Quaternary discontinuity) in the Gulf Cádiz and Porcupine Seabight and resulted from the fourth intensification stage of the MOW/AMW (Kano et al., 2007; Hernández-Molina et al., 2016; Lofi et al., 2016). The coldest Pleistocene time interval was recorded in the Mediterranean Sea at 474–427 ka (MIS 12) (Hughes et al., 2007), suggesting a dense MOW/AMW circulating along the NE Atlantic Ocean (Roque et al., 2012). This MOW/AMW circulation variability is recorded by the LQD erosional unconformity, in the Cádiz and Porcupine CDS (Van Rooij et al., 2007; Huvenne et al., 2009; Llave et al., 2011; Hernández-Molina et al., 2016), which displays similar seismic facies compared with H6 (Figs. 4, 5). As a result, H6 is tentatively correlated with the LQD.

5.2 Sedimentary evolution

Isochore maps and associated geological interpretation show distinctive depositional patterns and sedimentary processes within each unit (Fig. 10). Four stages of the Le Danois CDS Pliocene–Quaternary sedimentary evolution are identified related to variations of the bottom-current circulation. They are marked as onset (units 1 and 2, ~3.3 to 3.5-3.0 Ma), initial (unit 3, 3.5-3.0 to 2.5-2.1 Ma), intermediate (unit 4, 2.5-2.1 to 0.9-0.7 Ma) and drift-growth (units 5 and 6, 0.9-0.7 Ma to present day) stages (Fig. 11).

5.2.1 Onset Stage (Miocene-late Pliocene)

In the intraslope basin, Miocene to late Pliocene deposits of units 1 and 2 mainly filled in mini-basins located between buried structural highs (Figs. 10a, b, 11a). Buried structural highs and associated mini-basins were formed by compressional processes along the Cantabrian continental margin during the Eocene and Oligocene (Gallastegui et al., 2002; Zamora et al., 2017). Turbidite depositional systems intensively initiated since the early Miocene tectonic inversion along the northern Biscay margins (Bourillet et al., 2006). These turbidite systems were primarily fed by large rivers that originated from northern Europe (Auffret et al., 2003; Droz et al., 2003). In the southern Bay of Biscay, however, turbidite systems, sourced from the Cantabrian and Pyrenees mountains, started to generate in the Pliocene (Bourillet et al., 2006; Gaudin et al., 2006; Rumín-Caparrós et al., 2016). No channel-levee features or

turbidite fans are observed in the Miocene unit, indicating the absence of dominant turbidity currents. The lack of high-energy turbulent currents could lead to the predominant deposition of pelagic or hemipelagic sediments (Bowland, 1993; Soreghan et al., 1999), which possibly make up the sedimentary section of the Miocene unit.

The Miocene-Pliocene transition (horizon 2) marks a significant shift in sedimentary stacking pattern (Fig. 7). This transition is coeval with the onset of the MOW at ~5.33 Ma (Llave et al., 2011; van der Schee et al., 2016). After the onset, in the Gulf of Cádiz the first unit deposited during the early Pliocene is a contourite sheeted contourite drift (Llave et al., 2011; Brackenridge et al., 2013; Roque et al., 20212; Hernández-Molina et al., 2016). Similarly, in the Le Danois CDS no mounded contourite features are observed in unit 2 (Fig. 6a). As it was proposed for the Gulf of Cádiz, during the early Pliocene the MOW was weak, which could be the same situation in the Le Danois Bank region. Another alternative, to cause the absence of mounded contourite drifts in the Le Danois Bank region is the domination of the North Atlantic Deep Water (NADW). There is no evidence of contourite drifts during this time interval in Goban Spur and Porcupine Seabight (Van Rooij et al., 2007; Ledivet et al., 2016) which could be explained since the AMW was so weak that it has very little or non-influence on this margin. In addition, to that margin-wide tectonic tilting and erosive processes associated with the enhanced NADW dominated these regions during the early Pliocene (Stoker et al., 2005; Elliot et al., 2006). A distinct long-term rise of the MOW production in the NE Atlantic only occurred during the mid-Pliocene (at 3.5 Ma) (Khélif et al., 2009). Therefore, the AMW was relatively weak in the Le Danois Bank region during this stage. Along the southern base of the Le Danois Bank, the disrupted to semi-continuous chaotic internal structure of this seismic section could be linked to mass-transport deposits (Fig. 6c) that resulted from regional gravity and debris flows documented by Bourillet et al. (2006).

5.2.2 Initial Stage (late Pliocene-early Quaternary)

A significant change from hemipelagic muds to sediments affected by bottom currents is recognized in the early Pliocene unit of the Cádiz CDS (Van der Schee et al., 2016). This shift is evidently confirmed by the presence of sheeted drifts in the Gulf of Cádiz, indicating a progressive MOW enhancement after 4.0-4.2 Ma (Llave et al., 2011; Roque et al., 2012; Brackenridge et al., 2013; Hernández-Molina et al., 2016). In the study area, the initiation of mounded features of the Le Danois Drift (Figs. 10c, 11b) approximately started from the late Pliocene (3.5-3.0 Ma)

The initial stage of the Le Danois CDS is coeval with the enhanced stage of the AMW (~3.2-3.0 Ma; Hernández-Molina et al., 2014), which indicates effective interactions of the AMW and the Cantabrian continental margin since the late Pliocene. During the late Pliocene, the intensified AMW extended further north after exiting the Gulf of Cádiz and the earliest evidence of the AMW is dated at ~3.5-3.3 Ma in Goban Spur (Khélifi et al., 2009). Thus, compared with sediment records of the Gulf of Cádiz and Porcupine Seabight, the full domination of the AMW on the entire southwest European continental margin is set at ~3.5-3.0 Ma.

In unit 3, a moat feature is observed associated with Le Danois Drift along the southern base of the Le Danois Bank (Figs. 3, 9c). This feature indicates focused bottom-current dynamics during this stage. From units 3a to 3b, the mounded nature of the Le Danois Drift gradually increased. Variation in the geometry of contourite drifts implies different bottom-current conditions, whereas mounded geometry of drifts is associated with bottom currents with high velocities (Faugères and Stow, 2008; Stow et al., 2009). This temporal change of geometry, together with the presence of a moat, suggests a local AMW enhancement, which coincides with the late Pliocene dynamics of the MOW/AMW in the NE Atlantic (Rogerson et al., 2012; Hernández-Molina et al., 2014; Khélifi et al., 2014). During the onset of the widespread NHG, the southward advance of ice-sheets induced cold conditions in the Mediterranean and North Atlantic regions, favouring the formation of a dense MOW (Rasche Kleiven et al., 2002; Becker et al., 2006; Rohling et al., 2014). This variability of the MOW has been recorded by the Cádiz CDS with the presence of distinctive contourite channels and drifts that indicates pathways of the MOW (Roque et al., 2012). At the distal site of the AMW, enhanced circulation was accompanied by a flourishing CWC period in Porcupine Seabight (Huvenne et al., 2009). By comparing all these sites along the pathways of the MOW/AMW, the onset of the contourite stage, which is associated with the intermediate water mass, started from the late Pliocene along the southwest European continental margin.

5.2.3 Intermediate Stage (early Quaternary-middle Pleistocene)

Widely distributed wavy features in unit 4 indicate the possible generation of sediment waves (Fig. 3). The occurrence of sediment waves is generally linked to high energetic current flows, such as turbidity currents, bottom currents or internal waves (Howe, 1996; Marani et al., 1993; Lee et al., 2002; Wynn and Stow, 2002; Ribó et al., 2016; 2018). In the Le Danois Bank region, channel-levee features are observed in unit 4 (Figs. 6, 8), which indicates initiation of the Lastres canyon system and associated turbidity processes (Fig. 10d). Concentrated turbidity currents form sediment waves in canyon channels (Wynn et

al., 2000; 2002; Mulder and Alexander, 2001). Due to overspill, sediments could overtop the levee crest and sediment waves may occur on the backslope of levees (Normark et al., 2002; Kane et al., 2010). Sediment waves observed in the intraslope basin are not associated with the turbidite levees or positioned within canyon channels (Fig. 3). These sediment waves are about 8-11 km away from the Lastres canyon system (Fig. 10d). Similar bedforms, which are 60 km away from the channel axis, are observed offshore eastern Canada (Normandeau et al., 2019). These bedforms are generated by the interaction between contour currents and overspill (Normandeau et al., 2019). Therefore, the interaction between turbidity currents and contour currents could possibly be a genetic mechanism for these sediment waves.

Bottom currents are not likely responsible for the formation of these sediment waves either. Along the southern base of the Le Danois Bank, unit 4 has been eroded and the early Quaternary AMW pathway is unknown (Fig. 3). However, the presence of a moat in unit 3 documented the NW-SE trending pathway of the AMW during the previous stage (Fig. 10c). Due to the along-slope flowing nature of bottom currents and the orientation of slope morphology, a NW-SE trending AMW flow is suggested. This orientation is parallel to wave crests (NW-SE to W-E orientations) of sediment waves (Figs. 3, 9d), which does not fit with the oblique-perpendicular orientated relationship between flow directions and bottom-current induced sediment waves (Wynn and Masson, 2008).

Internal waves are another possibility for the occurrence of these sediment waves. During the early Quaternary glacial periods, the AMW core varied around 1500 m water depth and the MOW/AMW had less stratification due to intensive mixing with North Atlantic water masses (Lebreiro et al., 2015). Mixing of different water masses could significantly trigger the occurrence of pycnoclines, where internal waves propagate between layers of different densities (Pomar et al., 2012; Ribo et al., 2016). In the intraslope basin, sediment waves (positioned at 1500-1600 m) located at the depth interval of the glacial AMW during the early Quaternary. The related internal wave processes are capable of transporting and depositing sediments to generate these sediment waves in the Le Danois intraslope basin (Pomar et al., 2012; Ribó et al., 2016). During interglacial periods of this stage, AMW was well stratified and the core was too shallow (~1100 m; Lebreiro et al., 2015) to reach the seabed of the centre of the intraslope basin. The interface between AMW and LSW (1400-1700 m, Delivet et al., 2016), however, could have provided a favourable environment for the occurrence of internal waves, in turn generating sediment waves. Similar features are observed in Goban Spur, where the internal tide regime was promoted by bottom currents

and internal waves locating at the AMW/LSW interface induced the formation of sediment waves (positioned at 1300-1600 m) (White, 2006; White and Dorschel, 2010; Delivet et al., 2016). The scales of wave height and length, vertical position and time ranges of these sediment waves are correlated with ones in the study area, suggesting a similar formation mechanism. Compared with the Cádiz CDS, where only mounded contourite drifts were formed during the early Quaternary (Hernández-Molina et al., 2016), the occurrence of sediment waves in the Bay of Biscay indicates regional mixing processes within the glacial AMW and at the interglacial AMW/LSW interface.

At the end of the intermediate stage, sediments within the intraslope basin were largely eroded during the middle Pleistocene (Figs. 7, 8, 9d). Similar erosional surfaces are observed in most CDS and contourite drifts along the southwest European margins (Van Rooij et al., 2007; Llave et al., 2011). These extreme erosive pulses resulted from a dense, deep and enhanced circulation of the MOW/AMW during the MPT (Rohling et al., 2014; Hernández-Molina et al., 2016; Bahr et al., 2018). Intensification of the MOW/AMW may be coeval with the global cooling, sea-level fall, and a particularly strong MOW production from the Mediterranean Sea at these times (Roque et al., 2012; Rofi et al., 2016). Additionally, due to the vigorous AMW flow, previous slope irregularities above structural highs were significantly eroded in the intraslope basin (Fig. 11c). The gentle and open slope morphology, thus, provided a favourable condition for the wide distribution and growth of contourite drifts in the study area.

5.2.4 Drift growth Stage (middle Pleistocene to present day)

During the drift growth stage, the Le Danois CDS exhibited the most pronounced phase for drift development (Figs. 9e, f). Aside from the Le Danois Drift, the Gijón and Asturias Drifts with elongated, mounded and separated features started to generate along the southern boundary and at the centre of the intraslope basin (Figs. 5, 7). Associated moats have a distinctive morphology, indicating focused bottom currents along the upper continental slope and the Le Danois Bank during this stage.

In units 5 and 6, the vertical position of the Le Danois moat varied between 1.1 and 1.85 s TWT (900-1900 m). Based on the vertical glacial (1300-2000 m water depth) and interglacial (600-1000 m water depth) position of the AMW during this stage (Schönfeld and Zahn, 2000; Rogerson et al., 2005; Voelker et al., 2006), the Le Danois Drift was constructed by the AMW in both interglacial and glacial periods. The Gijón and the Asturias Moats, located at a shallower depth (400-1100 m), are beyond the reach of the glacial AMW and could only be generated during the interglacial climatic conditions. As such, due to the limited depth of the slope morphology, the denser glacial AMW, obstructed by the intraslope basin and

failed to penetrate along the seafloor of the basin, only flowed along the southern and northern flanks of the Le Danois Bank. During the interglacial intervals, however, the shallower AMW widely interacted with the entire intraslope basin.

In unit 6, a plastered drift (200-500 m), located within the depth intervals of the ENACW, is identified along the upper continental slope (Figs. 4, 9f). During the coldest Pleistocene time interval (MIS 12), the northward extension of the subtropical front resulted in the domination of the IPC and promoted the ENACW along the western and northern Iberian margins (Lambert et al., 2008; Voelker et al., 2015). Eventually, the effective interaction between the ENACW and the Le Danois upper continental slope generated plastered drifts from the late Quaternary onwards.

5.3 Modern versus past current patterns

Along the southern flank and the southeast base of the Le Danois Bank, two plastered drifts (1400-1920 m) are observed in unit 6 within the depth range of the present-day LSW (Figs. 7, 8, 9f). These two plastered drifts are located within the range of the present-day LSW. However, these two drifts could not be generated by the LSW. During the late Pleistocene, the polar front was located south of the Labrador Sea, which provided unfavourable conditions for the formation of the LSW (Venz et al., 1999). The stable LSW was established only during the early Holocene (Hillaire-Marcel et al., 2001; 2011). During the late Pleistocene, the dense glacial AMW penetrated at a great water depth between 1300-2000 m (Schönfeld and Zahn, 2000). The flow depth of glacial AMW can be compared with the present-day LSW. As such, modern current patterns do not necessarily relate to past contourite drift systems.

5.4 Sedimentary cycles and accumulation rates

In the Le Danois Drift, the sedimentary section of unit 5 displays distinctive repeated features. This cyclic pattern could be compared with the cyclicity observed in the upper sequences in the Cádiz CDS (Llave et al., 2001; Mestdagh et al., 2019) and the Porcupine CDS (Van Rooij et al., 2003). There, the period of low-frequency sedimentary cycles is registered in the range of 95–105 ky, coinciding with the periodicity of glacial/interglacial cycles (100 ky) of the earth since the middle Pleistocene (Elderfield et al., 2012; Lofi et al., 2016). In the Cádiz CDS, the acoustically transparent lower part and the moderate-high amplitude upper part respectively represent mud and sandy dominated sediments, indicating coarsening-upward sequences (Hernández-Molina et al., 2016; Lofi et al., 2016). This variation is linked to the intensity changes of the MOW/AMW during the interglacial to glacial periods (Rogerson et al., 2005;

Voelker et al., 2015). However, no similar cyclic features are observed in the Gijón and the Asturias drifts (Figs. 4, 6b, c). The difference in the internal structure of the drifts further supported that the Gijón and the Asturias drifts resulted from the interglacial-AMW. In unit 6 (after ~0.4 Ma), no cyclic features are shown in the entire Le Danois Bank region. Similar conditions are observed at IODP Site U1386 in the Cádiz CDS, where the upper MOW core was largely unaffected by glacial-interglacial climatic conditions between ~0.47 and ~0.13 Ma (Kaboth et al., 2017). These features could be related to the interplay of renewed tectonic activity and bottom-current circulation in the Gulf of Cádiz between MIS 13 and 11 (Hernández-Molina et al., 2016). Local salt movements are still active and significantly affect the present-day seafloor in the Algarve basin of the Gulf of Cádiz (Matias et al., 2017). Salt deformation can thus also create topographic obstacles on the seafloor and significantly change circulation patterns of the MOW.

The accumulation rates of the Le Danois CDS have been tentatively calculated based on the thickness of each unit, the related velocity model of time-depth conversion (Fig. 2b) and the tentative chronostratigraphy. During the onset stage, unit 3 (200-250 m thick) deposited within ~1 My. The estimated accumulation rate is about 25 cm/ky. During the intermediate stage, the least eroded strata of unit 4 (380 m thick) at the centre of the intraslope basin deposited within ~1.4 My, indicating a rate of at least ~27 cm/ky. During the subsequent growth-drift stage, estimated sedimentation rates of units 5 (50-75 m thick) and 6 (20-50 m thick) are namely within the range of 15-10 and 5-12.5 cm/ky. This characteristic of the Le Danois CDS is compatible with the one of the Cádiz CDS (Llave et al., 2001; Hernández-Molina et al., 2014), where accumulation rates significantly increased since late Pliocene times (~ 3.5-3.0Ma) (Llave et al., 2001; 2011; Hernández-Molina et al., 2016).

In the Cádiz CDS, increased sedimentation rates are coeval with the onset of the present-day contourite features, indicating higher volumes of MOW input into the Atlantic and a rise in sediment supply to offshore depocenters since the late Pliocene (Hernández-Molina et al., 2016). The NE Atlantic drifts, generated at the deep-water depth, developed since Miocene times and have maximum sedimentation rates during the early Pliocene (Hunter et al., 2007; Knutz, 2008; Müller-Michaelis et al., 2013). Large sediment supply from meltwater plumes along glacier margins and from high NADW production yielded higher sedimentation rates to NE Atlantic drifts during the warm Pliocene (Knutz, 2008). By comparing these areas, larger volumes of the intermediate water mass, instead of deep Atlantic water masses, highly influenced sediment transportation in the NE Atlantic from the late Pliocene onwards (Fig. 11).

6 Conclusion

The Pliocene-Quaternary variability of contourite features and depositional processes of the Le Danois CDS illustrate past bottom-current circulation patterns along the Cantabrian continental margin. During the early Pliocene the AMW was very weak and the effective interaction of it along the Cantabrian continental margin initiated during the late Pliocene (3.5-3.0 Ma). During the early Quaternary (2.5-0.9 Ma), internal waves resulted from turbulent mixing of water masses and induced development of sediment waves. During the middle Pleistocene (0.9-0.7 to ~0.47 Ma), The dense and deep AMW only flowed along the flank of the Le Danois Bank. The ENACW started to be involved in the generation of plastered drifts from the late Quaternary (~0.47 Ma) onwards.

The Gijón Drift, where no cyclic features were noted, was built only during the interglacial climatic conditions since the middle Pleistocene. The Le Danois Drift was built up by the AMW in both interglacial and glacial periods. Cyclic patterns with acoustically transparent lower parts and moderate-high amplitude upper parts are displayed in the middle Pleistocene units. These repeated depositional structures gradually thinned after the late Quaternary (~0.47 Ma). Sedimentation rates of the Le Danois CDS gradually increased since the late Pliocene and reached their maximum during the mid-Pleistocene. This variation in sedimentation rates suggests the domination of the intermediate water mass on sediment transport along the NE Atlantic continental margins from the late Pliocene (3.5-3.0 Ma) onwards.

Seafloor morphological features of the Le Danois CDS were previously linked with the present-day oceanography (Liu et al., 2019). However, the LSW was not involved in the build-up of contourite drifts during the past. The flowing depth of glacial AMW can be compared with the present-day LSW. As such, modern current patterns do not necessarily relate to ancient contourite drift systems. Therefore, past circulation patterns and flowing depth of water masses, as well as their response to paleoclimate variations, should be considered for future contourite studies.

Acknowledgements

This study was carried out within the framework of a Chinese Scholarship Council "CSC Grant" (201506410062). This study built on achievements of project ESF Euromargins MOUNDFORCE, EC FP5 RTN EURODOM and EC FP6 HERMES 626 (GOCE-CT-2005-511234-1). The research cruises namely framed within the ECOMARG (REN2002-624 00916/MAR) and MARCONI (REN2001-1734 C03-01/M)

projects. Shiptime RV Belgica was provided by BELSPO and RBINS–OD Nature. This study was conducted in collaboration with "The Drifters" Research Group of the Royal Holloway University of London (UK) and it is related to the projects CTM 2012-39599-C03, CGL2016-80445-R, and CTM2016-75129-C3-1-R (REN2001-1734 C03-01/M). It was also carried out in collaboration with the Continental Margins Group-GMC from ICM-CSIC (Spain) and its related Spanish projects (CTM2008-06399-C04-04/MAR; CTM2012-39599-CO3-O3; CMT2015- 65461-C2-R (MINEICO/FEDER).

Declaration of interests

The authors declare that they have no known competing financial interests or personal relationships that could have appeared to influence the work reported in this paper.

References

Alvarez-Marrón, J., Pérez-Estaún, A., Danñobeitia, J.J., Pulgar, J.A., Martínez, Catalán, J.R., Marcos, A., Bastida, F., Ayarza, Arribas, P., Aller, J., Gallart, A., Gonzalez-Lodeiro, F., Banda, E., Comas, M.C., Córdoba, D., 1996. Seismic structure of the northern continental margin of Spain from ESCIN deep seismic profiles. Tectonophysics 264, 153–174. http://dx.doi.org/10.1016/S0040-1951(96)00124-2

Auffret, G.A., Le Suavé, R., Garlan, T., Bourillet, J.F., Henriet, J.P., Zaragosi, S., Voisset, M., Lucas, S., 2003. The Celtic and Armorican Margins — a New View, in: Mienert, J., Weaver, P. (Eds.), European Margin Sediment Dynamics: Side-Scan Sonar and Seismic Images. Springer Berlin Heidelberg, Berlin, Heidelberg, pp. 223–228. https://doi.org/10.1007/978-3-642-55846-7_36

Bahr, A., Kaboth, S., Hodell, D., Zeeden, C., Fiebig, J., Friedrich, O., 2018. Oceanic heat pulses fueling moisture transport towards continental Europe across the mid-Pleistocene transition. Quaternary Science Reviews 179, 48-58. https://doi.org/10.1016/j.quascirev.2017.11.009

Becker, J., Lourens, L.J., Raymo, M.E., 2006. High-frequency climate linkages between the North Atlantic and the Mediterranean during marine oxygen isotope stage 100 (MIS100). Paleoceanography 21. https://doi.org/10.1029/2005PA001168

Bender, V.B., Hanebuth, T.J.J., Mena, A., Baumann, K.-H., Francés, G., von Dobeneck, T., 2012. Control of sediment supply, palaeoceanography and morphology on late Quaternary sediment dynamics at the Galician continental slope. Geo-Marine Lett. 32, 313–335. https://doi.org/10.1007/s00367-012-0282-2

Béthoux, J.-P., Pierre, C., 1999. Mediterranean functioning and sapropel formation: respective influences of climate and hydrological changes in the Atlantic and the Mediterranean. Mar. Geol. 153, 29–39. https://doi.org/10.1016/S0025-3227(98)00091-7

Boillot, G., Dupeuble, P.A., Malod, J., 1979. Subduction and tectonics on the continental margin off northern Spain. Mar. Geol. 32, 53–70. http://dx.doi.org/10.1016/0025-3227(79)90146-4

Bourillet, J.-F., Zaragosi, S., Mulder, T., 2006. The French Atlantic margin and deep-sea submarine systems. Geo-Marine Lett. 26, 311–315. https://doi.org/10.1007/s00367-006-0042-2

Bowland, C.L., 1993. Depositional history of the western Colombian Basin, Caribbean Sea, revealed by seismic stratigraphy. GSA Bull. 105, 1321–1343. https://doi.org/10.1130/0016-7606(1993)105<1321:DHOTWC>2.3.CO;2

Burton, K.W., Ling, H.-F., O'Nions, R.K., 1997. Closure of the Central American Isthmus and its effect on deep-water formation in the North Atlantic. Nature 386, 382. https://doi.org/10.1038/386382a0

Cadenas, P., Fernández-Viejo, G., 2017. The Asturian Basin within the North Iberian margin (Bay of Biscay): seismic characterisation of its geometry and its Mesozoic and Cenozoic cover. Basin Res. 29, 521–541. https://doi.org/10.1111/bre.12187

Catalán, J.R.M., Arenas, R., García, F.D. Cuadra, P.G., Gómez-Barreiro, J., Abati, J., Castiñeiras, P., Fernández-Suárez, J., Martínez, S.S., Andonaegui, P., Clavijo, E.G., Montes, A.D., Pascual, F.J.R., Aguado, B.V., 2007. Space and time in the tectonic evolution of the northwestern Iberian Massif: Implications for the Variscan belt. Geol. Soc. Am. Mem. 200, 403–423. https://doi.org/10.1130/2007.1200(21)

Collart, T., Verreydt, W., Hernandez-Molina, F.J., Llave, E., Leon, R., Gomez-Ballesteros, M., Pons-Branchu, E., Stewart, H., Van Rooij, D., 2018. Sedimentary processes and cold-water coral mini-mounds at the Ferrol canyon head, NW Iberian margin. Prog. Oceanogr. 169, 48–65. https://doi.org/10.1016/j.pocean.2018.02.027

Costa, S., Rey, P., 1995. Lower crustal rejuvenation and growth during post-thickening collapse: Insights from a crustal cross section through a Variscan metamorphic core complex. Geology 23, 905–908. https://doi.org/10.1130/0091-7613(1995)023<0905:LCRAGD>2.3.CO;2

Delivet, S., Van Eetvelt, B., Monteys, X., Ribó, M., Van Rooij, D., 2016. Seismic geomorphological reconstructions of Plio-Pleistocene bottom current variability at Goban Spur. Mar. Geol. 378, 261–275. http://dx.doi.org/10.1016/j.margeo.2016.01.001

Droz, L., Auffret, G.A., Savoye, B., 2003. The Celtic Deep-Sea Fan: Seismic Facies, Architecture and Stratigraphy, in: Mienert, J., Weaver, P. (Eds.), European Margin Sediment Dynamics: Side-Scan Sonar and Seismic Images. Springer Berlin Heidelberg, Berlin, Heidelberg, pp. 233–238. https://doi.org/10.1007/978-3-642-55846-7_38

Elderfield, H., Ferretti, P., Greaves, M., Crowhurst, S., McCave, I.N., Hodell, D., Piotrowski, A.M., 2012. Evolution of Ocean Temperature and Ice Volume Through the Mid-Pleistocene Climate Transition. Science 337, 704–709. https://doi.org/10.1126/science.1221294

Elliott, G.M., Shannon, P.M., Haughton, P.D.W., Praeg, D., O'Reilly, B., 2006. Mid- to Late Cenozoic canyon development on the eastern margin of the Rockall Trough, offshore Ireland. Mar. Geol. 229, 113–132. https://doi.org/10.1016/j.margeo.2006.03.008

Ercilla, G., Casas, D., Estrada, F., Vázquez, J.T., Iglesias, J., García, M., Gómez, M., Acosta, J., Gallart, J., Maestro-González, A., 2008. Morphosedimentary features and recent depositional architectural model of the Cantabrian continental margin. Mar. Geol. 247, 61–83. http://dx.doi.org/10.1016/j.margeo.2007.08.007

Ercilla, G., Casas, D., Vázquez, J.T., Iglesias, J., Somoza, L., Juan, C., Medialdea, T., León, R., Estrada, F., García-Gil, S., Farran, M. i., Bohoyo, F., García, M., Maestro, A., 2011. Imaging the recent sediment dynamics of the Galicia Bank region (Atlantic, NW Iberian Peninsula). Mar. Geophys. Res. 32, 99–126. https://doi.org/10.1007/s11001-011-9129-x

Faugères, J.-C., Gonthier, E., Mulder, T., Kenyon, N., Cirac, P., Griboulard, R., Berné, S., Lesuavé, R., 2002. Multi-process generated sediment waves on the Landes Plateau (Bay of Biscay, North Atlantic). Mar. Geol. 182, 279–302. http://dx.doi.org/10.1016/S0025-3227(01)00242-0

Flecker, R., Krijgsman, W., Capella, W., de Castro Martíns, C., Dmitrieva, E., Mayser, J.P., Marzocchi, A., Modestou, S., Ochoa, D., Simon, D., Tulbure, M., van den Berg, B., van der Schee, M., de Lange, G., Ellam, R., Govers, R., Gutjahr, M., Hilgen, F., Kouwenhoven, T., Lofi, J., Meijer, P., Sierro, F.J., Bachiri,

N., Barhoun, N., Alami, A.C., Chacon, B., Flores, J.A., Gregory, J., Howard, J., Lunt, D., Ochoa, M., Pancost, R., Vincent, S., Yousfi, M.Z., 2015. Evolution of the Late Miocene Mediterranean–Atlantic gateways and their impact on regional and global environmental change. Earth-Science Rev. 150, 365–392. https://doi.org/10.1016/j.earscirev.2015.08.007

Flesche Kleiven, H., Jansen, E., Fronval, T., Smith, T.M., 2002. Intensification of Northern Hemisphere glaciations in the circum Atlantic region (3.5–2.4 Ma) – ice-rafted detritus evidence. Palaeogeogr. Palaeoclimatol. Palaeoecol. 184, 213–223. https://doi.org/10.1016/S0031-0182(01)00407-2

Friedrich, O., Wilson, P.A., Bolton, C.T., Beer, C.J., Schiebel, R., 2013. Late Pliocene to early Pleistocene changes in the North Atlantic Current and suborbital-scale sea-surface temperature variability. Paleoceanography 28, 274–282. https://doi.org/doi:10.1002/palo.20029

Friocourt, Y., Levier, B., Speich, S., Blanke, B., Drijfhout, S.S., 2007. A regional numerical ocean model of the circulation in the Bay of Biscay. J. Geophys. Res. Ocean. 112. https://doi.org/10.1029/2006JC003935

Gallastegui, J., Pulgar, J.A., Gallart, J., 2002. Initiation of an active margin at the North Iberian continent-ocean transition. Tectonics 21, 14–15. https://doi.org/10.1029/2001TC901046

García, M., Hernández-Molina, F.J., Alonso, B., Vázquez, J.T., Ercilla, G., Llave, E., Casas, D., 2016. Erosive sub-circular depressions on the Guadalquivir Bank (Gulf of Cadiz): Interaction between bottom current, mass-wasting and tectonic processes. Mar. Geol. 378, 5–19. http://dx.doi.org/10.1016/j.margeo.2015.10.004

Gaudin, M., Mulder, T., Cirac, P., Berné, S., Imbert, P., 2006. Past and present sedimentary activity in the Capbreton Canyon, southern Bay of Biscay. Geo-Marine Lett. 26, 331. https://doi.org/10.1007/s00367-006-0043-1

González-Pola, C., Díaz del Río, G., Ruiz-Villarreal, M., Sánchez, R.F., Mohn, C., 2012. Circulation patterns at Le Danois Bank, an elongated shelf-adjacent seamount in the Bay of Biscay. Deep Sea Res. Part I Oceanogr. Res. Pap. 60, 7–21. http://dx.doi.org/10.1016/j.dsr.2011.10.001

Hayward, B.W., Sabaa, A.T., Kawagata, S., Grenfell, H.R., 2009. The Early Pliocene re-colonisation of the deep Mediterranean Sea by benthic foraminifera and their pulsed Late Pliocene–Middle

Pleistocene decline. Mar. Micropaleontol. 71, 97–112. https://doi.org/10.1016/j.marmicro.2009.01.008

Hebbeln, D., Van Rooij, D., Wienberg, C., 2016. Good neighbours shaped by vigorous currents: Cold-water coral mounds and contourites in the North Atlantic. Mar. Geol. 378, 171–185. http://dx.doi.org/10.1016/j.margeo.2016.01.014

Hernández-Molina, F.J., Serra, N., Stow, D.A. V, Llave, E., Ercilla, G., Van Rooij, D., 2011. Along-slope oceanographic processes and sedimentary products around the Iberian margin. Geo-Marine Lett. 31, 315–341. https://doi.org/10.1007/s00367-011-0242-2

Hernández-Molina, F.J., Llave, E., Preu, B., Ercilla, G., Fontan, A., Bruno, M., Serra, N., Gomiz, J.J., Brackenridge, R.E., Sierro, F.J., Stow, D.A. V, García, M., Juan, C., Sandoval, N., Arnaiz, A., 2014. Contourite processes associated with the Mediterranean Outflow Water after its exit from the Strait of Gibraltar: Global and conceptual implications. Geology 42, 227–230. https://doi.org/10.1130/g35083.1

Hernández-Molina, F.J., Sierro, F.J., Llave, E., Roque, C., Stow, D.A. V, Williams, T., Lofi, J., Van der Schee, M., Arnáiz, A., Ledesma, S., Rosales, C., Rodríguez-Tovar, F.J., Pardo-Igúzquiza, E., Brackenridge, R.E., 2016. Evolution of the gulf of Cadiz margin and southwest Portugal contourite depositional system: Tectonic, sedimentary and paleoceanographic implications from IODP expedition 339. Mar. Geol. 377, 7–39. http://dx.doi.org/10.1016/j.margeo.2015.09.013

Hillaire-Marcel, C., Bilodeau, G., 2000. Instabilities in the Labrador Sea water mass structure during the last climatic cycle. Can. J. Earth Sci. 37, 795–809. https://doi.org/10.1139/e99-108

Hillaire-Marcel, C., de Vernal, A., Bilodeau, G., Weaver, A.J., 2001. Absence of deep-water formation in the Labrador Sea during the last interglacial period. Nature 410, 1073. https://doi.org/10.1038/35074059

Hillaire-Marcel, C., de Vernal, A., McKay, J., 2011. Foraminifer isotope study of the Pleistocene Labrador Sea, northwest North Atlantic (IODP Sites 1302/03 and 1305), with emphasis on paleoceanographical differences between its “inner” and “outer” basins. Mar. Geol. 279, 188–198. https://doi.org/10.1016/j.margeo.2010.11.001

Howe, J.A., 1996. Turbidite and contourite sediment waves in the northern Rockall Trough, North Atlantic Ocean. Sedimentology 43, 219–234. https://doi.org/10.1046/j.1365-3091.1996.d01-1.x

Hughes, P.D., Woodward, J.C., Gibbard, P.L., 2007. Middle Pleistocene cold stage climates in the Mediterranean: New evidence from the glacial record. Earth Planet. Sci. Lett. 253, 50–56. https://doi.org/10.1016/j.epsl.2006.10.019

Hunter, S.E., Wilkinson, D., Stanford, J., Stow, D.A. V, Bacon, S., Akhmetzhanov, A.M., Kenyon, N.H., 2007. The Eirik Drift: a long-term barometer of North Atlantic deepwater flux south of Cape Farewell, Greenland. Geol. Soc. London, Spec. Publ. 276, 245. https://doi.org/10.1144/GSL.SP.2007.276.01.12

Huvenne, V.A.I., Van Rooij, D., De Mol, B., Thierens, M., O'Donnell, R., Foubert, A., 2009. Sediment dynamics and palaeo-environmental context at key stages in the Challenger cold-water coral mound formation: Clues from sediment deposits at the mound base. Deep Sea Res. Part I Oceanogr. Res. Pap. 56, 2263–2280. http://dx.doi.org/10.1016/j.dsr.2009.08.003

Iglesias, J., 2009. Sedimentation on the cantabrian continental margin from late oligocene to quaternary. Unpubl. PhD Thesis.

Iorga, M.C., Lozier, M.S., 1999. Signatures of the Mediterranean outflow from a North Atlantic climatology 1. Salinity and density fields. J. Geophys. Res. 104, 25985–26009. https://doi.org/10.1029/1999JC900115

Jia, Y., Coward, A.C., de Cuevas, B.A., Webb, D.J., Drijfhout, S.S., 2007. A Model Analysis of the Behavior of the Mediterranean Water in the North Atlantic. J. Phys. Oceanogr. 37, 764–786. https://doi.org/10.1175/JPO3020.1

Kaboth, S., Bahr, A., Reichart, G.-J., Jacobs, B., Lourens, L.J., 2016. New insights into upper MOW variability over the last 150 kyr from IODP 339 Site U1386 in the Gulf of Cadiz. Mar. Geol. 377, 136–145. http://dx.doi.org/10.1016/j.margeo.2015.08.014

Kaboth, Stefanie, de Boer, B., Bahr, A., Zeeden, C., Lourens, L.J., 2017. Mediterranean Outflow Water dynamics during the past ~570 kyr: Regional and global implications. Paleoceanography 32, 634–647. https://doi.org/10.1002/2016PA003063

Kane, I.A., McCaffrey, W.D., Peakall, J., Kneller, B.C., 2010. Submarine channel levee shape and sediment waves from physical experiments. Sediment. Geol. 223, 75–85. https://doi.org/10.1016/j.sedgeo.2009.11.001

Kano, A., Ferdelman, T.G., Williams, T., Henriet, J.-P., Ishikawa, T., Kawagoe, N., Takashima, C., Kakizaki, Y., Abe, K., Sakai, S., Browning, E.L., Li, X., 2007. Age constraints on the origin and growth history of a deep-water coral mound in the northeast Atlantic drilled during Integrated Ocean Drilling Program Expedition 307. Geology 35, 1051–1054. https://doi.org/10.1130/G23917A.1

Khélifi, N., Sarnthein, M., Andersen, N., Blanz, T., Frank, M., Garbe-Schönberg, D., Haley, B.A., Stumpf, R., Weinelt, M., 2009. A major and long-term Pliocene intensification of the Mediterranean outflow, 3.5–3.3 Ma ago. Geology 37, 811–814. https://doi.org/10.1130/G30058A.1

Khélifi, N., Sarnthein, M., Frank, M., Andersen, N., Garbe-Schönberg, D., 2014. Late Pliocene variations of the Mediterranean outflow. Mar. Geol. 357, 182–194. http://dx.doi.org/10.1016/j.margeo.2014.07.00[illegible]

Knutz, P.C., 2008. Chapter 24 Palaeoceanographic Significance of Contourite Drifts, in: Rebesco, M., Camerlenghi, A. (Eds.), Developments in Sedimentology. Elsevier, pp. 511–535. http://dx.doi.org/10.1016/S0070-4571(08)10024-3

Knutz, P.C., Hopper, J.R., Gregersen, U., Nielsen, T., Japsen, P., 2015. A contourite drift system on the Baffin Bay–West Greenland margin linking Pliocene Arctic warming to poleward ocean circulation. Geology 43, 907–910. https://doi.org/10.1130/G36927.1

Lambert, F., Delmonte, B., Petit, J.R., Bigler, M., Kaufmann, P.R., Hutterli, M.A., Stocker, T.F., Ruth, U., Steffensen, J.P., Maggi, V., 2008. Dust-climate couplings over the past 800,000 years from the EPICA Dome C ice core. Nature 452, 616. https://doi.org/10.1038/nature06763

Lavín, A., Valdés, L., Sánchez, F., Abaunza, P., Forest, A., Boucher, J., Lazure, P., Jegou, A.M., 2006. The Bay of Biscay: the encountering of the ocean and the shelf, in: Brink, A.R.R.K.H. (Ed.), The Sea. the President and Fellows of Harvard College, pp. 933–999.

Lebreiro, S.M., Antón, L., Reguera, M.I., Fernández, M., Conde, E., Barrado, A.I., Yllera, A., 2015. Zooming into the Mediterranean outflow fossil moat during the 1.2–1.8 million years period (Early-

Pleistocene) - An approach by radiogenic and stable isotopes. Glob. Planet. Change 135, 104–118. https://doi.org/10.1016/j.gloplacha.2015.10.010

Lee, H.J., Syvitski, J.P.M., Parker, G., Orange, D., Locat, J., Hutton, E.W.H., Imran, J., 2002. Distinguishing sediment waves from slope failure deposits: field examples, including the 'Humboldt slide', and modelling results. Mar. Geol. 192, 79–104. http://dx.doi.org/10.1016/S0025-3227(02)00550-9

Lisiecki, L.E., Raymo, M.E., 2005. A Pliocene-Pleistocene stack of 57 globally distributed benthic δ18O records. Paleoceanography 20. https://doi.org/10.1029/2004PA001071

Liu, S., Van Rooij, D., Vandorpe, T., González-Pola, C., Ercilla, G., Hernández-Molina, F.J., 2019. Morphological features and associated bottom-current dynamics in the Le Danois Bank region (southern Bay of Biscay, NE Atlantic): A model in a topographically constrained small basin. Deep Sea Res. Part I Oceanogr. Res. Pap. https://doi.org/10.1016/j.dsr.2019.05.014

Llave, E., Hernandez-Molina, F.J., Somoza, L., Diaz-del Rio, V., Stow, D.A. V, Maestro, A., Alveirinho Dias, J.M., 2001. Seismic stacking pattern of the Faro-Albufeira contourite system (Gulf of Cadiz): a Quaternary record of paleoceanographic and tectonic influences. Mar. Geophys. Res. 22, 487–508. https://doi.org/10.1023/A:1016355201344

Llave, E., Schönfeld, J., Hernandez-Molina, F.J., Mulder, T., Somoza, L., Diaz-del Rio, V., Sanchez-Almazo, I., 2006. High-resolution stratigraphy of the Mediterranean outflow contourite system in the Gulf of Cadiz during the late Pleistocene: The impact of Heinrich events. Mar. Geol. 277, 241–262. https://doi.org/10.1016/j.margeo.2005.11.015

Llave, E., Matias, H., Hernandez-Molina, F.J., Ercilla, G., Stow, D.A. V, Medialdea, T., 2011. Pliocene-Quaternary contourites along the northern Gulf of Cadiz margin: sedimentary stacking pattern and regional distribution. Geo-Marine Lett. 31, 377–390. https://doi.org/10.1007/s00367-011-0241-3

Lofi, J., Voelker, A.H.L., Ducassou, E., Hernández-Molina, F.J., Sierro, F.J., Bahr, A., Galvani, A., Lourens, L.J., Pardo-Igúzquiza, E., Pezard, P., Rodríguez-Tovar, F.J., Williams, T., 2016. Quaternary chronostratigraphic framework and sedimentary processes for the Gulf of Cadiz and Portuguese

Contourite Depositional Systems derived from Natural Gamma Ray records. Mar. Geol. 377, 40–57. https://doi.org/10.1016/j.margeo.2015.12.005

Marani, M., Argnani, A., Roveri, M., Trincardi, F., 1993. Sediment drifts and erosional surfaces in the central Mediterranean: seismic evidence of bottom-current activity. Sediment. Geol. 82, 207–220. https://doi.org/10.1016/0037-0738(93)90122-L

Maslin, M.A., Ridgwell, A.J., 2005. Mid-Pleistocene revolution and the 'eccentricity myth.' Geol. Soc. London, Spec. Publ. 247, 19–34. https://doi.org/10.1144/gsl.sp.2005.247.01.02

Matias, H., Kress, P., Terrinha, P., Mohriak, W., Menezes, P. T. L., Matias, L., Santos, F., Sandnes, F., 2011. Salt tectonics in the western Gulf of Cádiz, southwest Iberia. AAPG Bulletin, 95(10), 1667–1698. doi:10.1306/01271110032

Mena, A., Francés, G., Pérez-Arlucea, M., Hanebuth, T.J.J., Bender, V.B., Nombela, M.A., 2018. Evolution of the Galicia Interior Basin over the last 60 ka: sedimentary processes and palaeoceanographic implications. J. Quat. Sci. 33, 536–549. https://doi.org/doi:10.1002/jqs.3032

Mulder, T., Alexander, J., 2001. The physical character of subaqueous sedimentary density flows and their deposits. Sedimentology 48, 269–299. https://doi.org/10.1046/j.1365-3091.2001.00360.x

Mulder, T., Zaragosi, S., Garlan, T., Mavel, J., Cremer, M., Sottolichio, A., Sénéchal, N., Schmidt, S., 2012. Present deep-submarine canyons activity in the Bay of Biscay (NE Atlantic). Mar. Geol. 295–298, 113–127. http://dx.doi.org/10.1016/j.margeo.2011.12.005

Müller-Michaelis, A., Uenzelmann-Neben, G., Stein, R., 2013. A revised Early Miocene age for the instigation of the Eirik Drift, offshore southern Greenland: Evidence from high-resolution seismic reflection data. Mar. Geol. 340, 1–15. https://doi.org/10.1016/j.margeo.2013.04.012

Normandeau, A., Campbell, D.C. and Cartigny, M.J., 2019. The influence of turbidity currents and contour currents on the distribution of deep-water sediment waves offshore eastern Canada. Sedimentology, 66(5), pp.1746-1767. https://doi.org/10.1111/sed.12557

Normark, W.R., Piper, D.J.W., Posamentier, H., Pirmez, C., Migeon, S., 2002. Variability in form and growth of sediment waves on turbidite channel levees. Mar. Geol. 192, 23–58. https://doi.org/10.1016/S0025-3227(02)00548-0

Pingree, R.D., Le Cann, B., 1990. Structure, strength and seasonality of the slope currents in the Bay of Biscay region. J. Mar. Biol. Assoc. United Kingdom 70, 857–885. https://doi.org/10.1017/S0025315400059117

Pomar, L., Morsilli, M., Hallock, P., Bádenas, B., 2012. Internal waves, an under-explored source of turbulence events in the sedimentary record. Earth-Science Rev. 111, 56–81. http://dx.doi.org/10.1016/j.earscirev.2011.12.005

Raddatz, J., Rüggeberg, A., Margreth, S., Dullo, W.-C., 2011. Paleoenvironmental reconstruction of Challenger Mound initiation in the Porcupine Seabight, NE Atlantic. Mar. Geol. 282, 79–90. https://doi.org/10.1016/j.margeo.2010.10.019

Raymo, M.E., Oppo, D.W., Flower, B.P., Hodell, D.A., McManus, J.F., Venz, K.A., Kleiven, K.F., McIntyre, K., 2004. Stability of North Atlantic water masses in face of pronounced climate variability during the Pleistocene. Paleoceanography 19. https://doi.org/doi:10.1029/2003PA000921

Rebesco, M., Camerlenghi, A., Van Loon, A.J., 2008. Chapter 1 Contourite Research: A Field in Full Development, in: Rebesco, M., Camerlenghi, A. (Eds.), Developments in Sedimentology. Elsevier, pp. 1–10. http://dx.doi.org/10.1016/S0070-4571(08)10001-2

Rebesco, M., Hernández-Molina, F.J., Van Rooij, D., Wåhlin, A., 2014. Contourites and associated sediments controlled by deep-water circulation processes: State-of-the-art and future considerations. Mar. Geol. 352, 111–154. https://doi.org/http://dx.doi.org/10.1016/j.margeo.2014.03.011

Reveillaud, J., Freiwald, A., Van Rooij, D., Le Guilloux, E., Altuna, A., Foubert, A., Vanreusel, A., Roy, K.O.L., Henriet, J.P., 2008. The distribution of scleractinian corals in the Bay of Biscay, NE Atlantic. Facies 54, 317–331. https://doi.org/10.1007/s10347-008-0138-4

Ribó, M., Puig, P., Muñoz, A., Lo Iacono, C., Masqué, P., Palanques, A., Acosta, J., Guillén, J., Gómez Ballesteros, M., 2016. Morphobathymetric analysis of the large fine-grained sediment waves over the Gulf of Valencia continental slope (NW Mediterranean). Geomorphology 253, 22–37. http://dx.doi.org/10.1016/j.geomorph.2015.09.027

Ribó, M., Durán, R., Puig, P., Van Rooij, D., Guillén, J., Masqué, P., 2018. Large sediment waves over the Gulf of Roses upper continental slope (NW Mediterranean). Mar. Geol. 399, 84–96. https://doi.org/10.1016/j.margeo.2018.02.006

Ries, A.C., 1978. The opening of the Bay of Biscay - a review. Earth-Science Rev. 14, 35–63. http://dx.doi.org/10.1016/0012-8252(78)90041-7

Rogerson, M., Rohling, E.J., Weaver, P.P.E., Murray, J.W., 2005. Glacial to interglacial changes in the settling depth of the Mediterranean Outflow plume. Paleoceanography 20. https://doi.org/10.1029/2004PA001106

Rogerson, M., Colmenero-Hidalgo, E., Levine, R.C., Rohling, E.J., Voelker, A.H.L., Bigg, G.R., Schönfeld, J., Cacho, I., Sierro, F.J., Löwemark, L., Reguera, M.I., de Abreu, L., Garrick, K., 2010. Enhanced Mediterranean-Atlantic exchange during Atlantic freshening phases. Geochemistry, Geophys. Geosystems 11. https://doi.org/10.1029/2009GC002931

Rogerson, M., Bigg, G.R., Rohling, E.J., Ramirez, J., 2012. Vertical density gradient in the eastern North Atlantic during the last 30,000 years. Clim. Dyn. 39, 589–598. https://doi.org/10.1007/s00382-011-1148-4

Rohling, E.J., Foster, G.L., Grant, K.M., Marino, G., Roberts, A.P., Tamisiea, M.E., Williams, F., 2014. Sea-level and deep-sea-temperature variability over the past 5.3 million years. Nature 508, 477–482. https://doi.org/10.1038/nature13230

Roque, C., Duarte, H., Terrinha, P., Valadares, V., Noiva, J., Cachão, M., Ferreira, J., Legoinha, P., Zitellini, N., 2012. Pliocene and Quaternary depositional model of the Algarve margin contourite drifts (Gulf of Cadiz, SW Iberia): Seismic architecture, tectonic control and paleoceanographic insights. Mar. Geol. 303–306, 42–62. http://dx.doi.org/10.1016/j.margeo.2011.11.001

Rumín-Caparrós, A., Sanchez-Vidal, A., González-Pola, C., Lastras, G., Calafat, A., Canals, M., 2016. Particle fluxes and their drivers in the Avilés submarine canyon and adjacent slope, central Cantabrian margin, Bay of Biscay. Prog. Oceanogr. 144, 39–61. http://dx.doi.org/10.1016/j.pocean.2016.03.004

Schönfeld, J., Zahn, R., 2000. Late Glacial to Holocene history of the Mediterranean Outflow. Evidence from benthic foraminiferal assemblages and stable isotopes at the Portuguese margin. Palaeogeogr. Palaeoclimatol. Palaeoecol. 159, 85–111. http://dx.doi.org/10.1016/S0031-0182(00)00035-3

Soreghan, M.J., Scholz, C.A., Wells, J.T., 1999. Coarse-grained, deep-water sedimentation along a border fault margin of Lake Malawi, Africa; seismic stratigraphic analysis. J. Sediment. Res. 69, 832–846. https://doi.org/10.2110/jsr.69.832

Stoker, M.S., Hoult, R.J., Nielsen, T., Hjelstuen, B.O., Laberg, J.S., Shannon, P.M., Praeg, D., Mathiesen, A., van Weering, T.C.E., McDonnell, A., 2005. Sedimentary and oceanographic responses to early Neogene compression on the NW European margin. Mar. Pet. Geol. 22, 1031–1044. https://doi.org/10.1016/j.marpetgeo.2005.01.009

Stow, D.A. V, Faugères, J.C., 2008. Chapter 13 Contourite Facies and the Facies Model, in: Rebesco, M., Camerlenghi, A. (Eds.), Developments in Sedimentology. Elsevier, pp. 223–256. http://dx.doi.org/10.1016/S0070-4571(08)10013-9

Stow, D.A. V, Javier Hernández-Molina, F., Llave, E., Sayago, M., 2009. Bedform-velocity matrix: The estimation of bottom current velocity from bedform observations. Geology 37, 327–330. https://doi.org/10.1130/G25259A.1

Teixeira, M., Terrinha, P., Roque, C., Rosa, M., Ercilla, G., Casas, D., 2019. Interaction of alongslope and downslope processes in the Alentejo Margin (SW Iberia) – Implications on slope stability. Mar. Geol. 410, 88–108. https://doi.org/10.1016/j.margeo.2018.12.011

Thierens, M., Browning, E., Pirlet, H., Loutre, M.F., Dorschel, B., Huvenne, V.A.I., Titschack, J., Colin, C., Foubert, A., Wheeler, A.J., 2013. Cold-water coral carbonate mounds as unique palaeo-archives: the Plio-Pleistocene Challenger Mound record (NE Atlantic). Quat. Sci. Rev. 73, 14–30. https://doi.org/10.1016/j.quascirev.2013.05.006

Toucanne, S., Zaragosi, S., Bourillet, J.F., Naughton, F., Cremer, M., Eynaud, F., Dennielou, B., 2008. Activity of the turbidite levees of the Celtic-Armorican margin (Bay of Biscay) during the last 30,000 years: Imprints of the last European deglaciation and Heinrich events. Mar. Geol. 247, 84–103. https://doi.org/10.1016/j.margeo.2007.08.006

Tugend, J., Manatschal, G., Kusznir, N. J., Masini, E., Mohn, G., & Thinon, I., 2014. Formation and deformation of hyperextended rift systems: Insights from rift domain mapping in the Bay of Biscay-Pyrenees. Tectonics, 33, 1239–1276. http://dx.doi.org/10.1002/2014TC003529

van Aken, H.M., 2000a. The hydrography of the mid-latitude northeast Atlantic Ocean: I: The deep water masses. Deep Sea Res. Part I Oceanogr. Res. Pap. 47, 757–788. http://dx.doi.org/10.1016/S0967-0637(99)00092-8

van Aken, H.M., 2000b. The hydrography of the mid-latitude Northeast Atlantic Ocean: II: The intermediate water masses. Deep Sea Res. Part I Oceanogr. Res. Pap. 47, 789–824. http://dx.doi.org/10.1016/S0967-0637(99)00112-0

van der Schee, M., Sierro, F., Jimenez-Espejo, F., Hernández-Molina, F., Flecker, R., Flores, J., Acton, G., Gutjahr, M., Grunert, P., García-Gallardo, A., 2016, Evidence of early bottom water current flow after the Messinian Salinity Crisis in the Gulf of Cadiz: Marine Geology, v. 380, p. 315-329, http://doi:10.1016/j.margeo.2016.04.005.

Van Rooij, D., De Mol, B., Huvenne, V., Ivanov, M., Henriet, J.P., 2003. Seismic evidence of current-controlled sedimentation in the Belgica mound province, upper Porcupine slope, southwest of Ireland. Mar. Geol. 195, 31–53. http://dx.doi.org/10.1016/S0025-3227(02)00681-3

Van Rooij, D., Blamart, D., Kozachenko, M., Henriet, J.-P., 2007. Small mounded contourite drifts associated with deep-water coral banks, Porcupine Seabight, NE Atlantic Ocean. Geol. Soc. London, Spec. Publ. 276, 225–244. https://doi.org/10.1144/gsl.sp.2007.276.01.11

Van Rooij, D., Iglesias, J., Hernández-Molina, F.J., Ercilla, G., Gomez-Ballesteros, M., Casas, D., Llave, E., De Hauwere, A., Garcia-Gil, S., Acosta, J., Henriet, J.P., 2010. The Le Danois Contourite Depositional System: Interactions between the Mediterranean Outflow Water and the upper Cantabrian slope (North Iberian margin). Mar. Geol. 274, 1–20. http://dx.doi.org/10.1016/j.margeo.2010.03.001

Venz, K.A., Hodell, D.A., Stanton, C., Warnke, D.A., 1999. A 1.0 Myr Record of Glacial North Atlantic Intermediate Water Variability from ODP Site 982 in the Northeast Atlantic. Paleoceanography 14, 42–52. https://doi.org/doi:10.1029/1998PA900013

Vissers, R.L.M., Meijer, P.T., 2012. Iberian plate kinematics and Alpine collision in the Pyrenees. Earth-Science Rev. 114, 61–83. https://doi.org/10.1016/j.earscirev.2012.05.001

Voelker, A.H.L., Lebreiro, S.M., Schönfeld, J., Cacho, I., Erlenkeuser, H., Abrantes, F., 2006. Mediterranean outflow strengthening during northern hemisphere coolings: A salt source for the glacial Atlantic? Earth Planet. Sci. Lett. 245, 39–55. http://dx.doi.org/10.1016/j.epsl.2006.03.014

Voelker, A.H.L., Salgueiro, E., Rodrigues, T., Jimenez-Espejo, F.J., Bahr, A., Alberto, A., Loureiro, I., Padilha, M., Rebotim, A., Röhl, U., 2015. Mediterranean Outflow and surface water variability off southern Portugal during the early Pleistocene: A snapshot at Marine Isotope Stages 29 to 34 (1020–1135ka). Glob. Planet. Change 133, 223–237. https://doi.org/10.1016/j.gloplacha.2015.08.015

Volkov, D.L., Fu, L.L., 2010. On the Reasons for the Formation and Variability of the Azores Current. J. Phys. Oceanogr. 40, 2197–2220. https://doi.org/10.1175/2010JPO4326.1

Weaver, P.P.E., Wynn, R.B., Kenyon, N.H., Evans, J., 2000. Continental margin sedimentation, with special reference to the north-east Atlantic margin. Sedimentology 47, 239–256. https://doi.org/doi:10.1046/j.1365-3091.2000.0470s1239.x

White, M., 2006. Benthic dynamics at the carbonate mound regions of the Porcupine Sea Bight continental margin. Int. J. Earth Sci. 96, 1. https://doi.org/10.1007/s00531-006-0099-1

White, M., Dorschel, B., 2010. The importance of the permanent thermocline to the cold water coral carbonate mound distribution in the NE Atlantic. Earth Planet. Sci. Lett. 296, 395–402. https://doi.org/10.1016/j.epsl.2010.05.025

Wold, C.N., 1994. Cenozoic sediment accumulation on drifts in the northern North Atlantic. Paleoceanography, 9(6), pp.917-941. https://doi.org/10.1029/94PA01438

Wynn, R.B., Weaver, P.P.E., Ercilla, G., Stow, D.A. V, Masson, D.G., 2000. Sedimentary processes in the Selvage sediment-wave field, NE Atlantic: new insights into the formation of sediment waves by turbidity currents. Sedimentology 47, 1181–1197. https://doi.org/10.1046/j.1365-3091.2000.00348.x

Wynn, R.B., Piper, D.J.W., Gee, M.J.R., 2002. Generation and migration of coarse-grained sediment waves in turbidity current channels and channel–lobe transition zones. Mar. Geol. 192, 59–78. https://doi.org/10.1016/S0025-3227(02)00549-2

Wynn, R.B., Masson, D.G., 2008. Chapter 15 Sediment Waves and Bedforms, in: Rebesco, M., Camerlenghi, A. (Eds.), Developments in Sedimentology. Elsevier, pp. 289–300. http://dx.doi.org/10.1016/S0070-4571(08)10015-2

Zamora, G., Fleming, M., Gallastegui, J., 2017. Chapter 16 - Salt Tectonics Within the Offshore Asturian Basin: North Iberian Margin, in: Soto, J.I., Flinch, J.F., Tari, G. (Eds.), Permo-Triassic Salt Provinces of Europe, North Africa and the Atlantic Margins. Elsevier, pp. 353–368. https://doi.org/10.1016/B978-0-12-809417-4.00017-3

Figures

Fig. 1. (a) Map of the Le Danois Bank area with the indication of: morphological domains and pathways of the Eastern North Atlantic Central Water (ENACW), the Atlantic Mediterranean Water (AMW) and the Labrador Sea Water (LSW); (b) Tectonic structure modified from Roca et al. (2011). The location of this cross-section is shown in the morphological map (a). The depth of water masses is derived from González-Pola et al., (2012).

Fig. 2. (a) Dataset map (contour lines every 100 m) indicating locations of single channel sparker and multi-channel airgun seismic profiles, as well as the position of Well MC H1-X (Cadenas and Fernandez-Viejo, 2016); (b) Time to depth conversion, which is derived from the borehole data (Well MC H-1X; Cadenas and Fernandez-Viejo, 2017); (c) High-resolution bathymetric map with indication of the regional geographic and morphological domains.

Fig. 3. Seismic stratigraphic framework of the Le Danois Bank region. Timing of major unconformities are compared with significant hiatuses of the NE Atlantic. Sea-level changes and accumulation rates of the NE Atlantic drifts are indicated as well. Abbreviations for discontinuities (from bottom to top): M=Miocene–Pliocene boundary; LPD=late Pliocene discontinuity; EQD=early Quaternary discontinuity; MPD=mid Pleistocene discontinuity; LQD=late Quaternary discontinuity.

Fig. 4. Single channel sparker seismic profile and the interpretation, showing 5 units (U2-U6) and associated subunits from the bottom to the top. Relative scales of depositional cycles are indicated by the size of red triangles. Seismic terminations are indicated by red arrows. The location of this seismic line is displayed in Fig. 2a. H2=the Miocene top (~5.33 Ma; dark blue dotted line); H3=late Pliocene discontinuity (~3.5-3.0 Ma; light blue dotted line); H4=early Quaternary discontinuity (~2.5-2.1 Ma; green dotted line); H5=mid Pleistocene discontinuity (~0.9-0.7 Ma; orange dotted line); H6=late Quaternary discontinuity (~0.47 Ma; red dotted line).

Fig. 5. Single channel sparker seismic profile and the interpretation, showing 5 units (U2-U6) and associated subunits from the bottom to the top. Relative scales of depositional cycles are indicated by the size of red triangles. Seismic terminations are indicated by red arrows. These cyclic features are coeval with glacial/interglacial climate cycles, which are displayed by the Marine Isotope Stage (MIS) and the benthic $\delta^{18}O$ and are derived from Lisiecki and Raymo (2005). The location of this seismic line is displayed in Fig. 2a. H2=the Miocene top (~5.33 Ma; dark blue dotted line); H3=late Pliocene discontinuity (~3.5-3.0 Ma; light blue dotted line); H4=early Quaternary discontinuity (~2.5-2.1 Ma; green dotted line); H5=mid

Pleistocene discontinuity (~0.9-0.7 Ma; orange dotted line); H6=late Quaternary discontinuity (~0.47 Ma; red dotted line).

Fig. 6. Multi-channel airgun (a) with higher-resolution sections obtained through a single channel sparker (b, c) seismic profile and the interpretation. The boundary of the Miocene-Quaternary and the Eocene-Oligocene units, which is derived from the borehole data (Well MC H1-X), is tentatively correlated with horizon 1. The core recovery is shown as well. Relative scales of depositional cycles are indicated by the size of red triangles. Seismic terminations are indicated by red arrows. The location of this seismic line is displayed in Fig. 2a. H1= the Miocene base (black dotted line); H2=the Miocene top (~5.33 Ma; dark blue dotted line); H3=late Pliocene discontinuity (~3.5-3.0 Ma; light blue dotted line); H4=early Quaternary discontinuity (~2.5-2.1 Ma; green dotted line); H5=mid Pleistocene discontinuity (~0.9-0.7 Ma; orange dotted line); H6=late Quaternary discontinuity (~0.47 Ma; red dotted line).

Fig. 7. Pseudo-3D model of the Gijón and Le Danois Drifts using multi-channel airgun seismic profiles, showing 6 units (U1-U6) from the bottom to the top. Locations of these seismic data are indicated in the slope gradient map. H1= the Miocene base (black dotted line); H2=the Miocene top (~5.33 Ma; dark blue dotted line); H3=late Pliocene discontinuity (~3.5-3.0 Ma; light blue dotted line); H4=early Quaternary discontinuity (~2.5-2.1 Ma; green dotted line); H5=mid Pleistocene discontinuity (~0.9-0.7 Ma; orange dotted line); H6=late Quaternary discontinuity (~0.47 Ma; red dotted line).

Fig. 8. Multi-channel airgun seismic profile and the interpretation, showing 6 units (U1-U6) from the bottom to the top. Seismic terminations are indicated by red arrows. The location of this seismic line is displayed in Fig. 2a. H1= the Miocene base (black dotted line); H2=the Miocene top (~5.33 Ma; dark blue dotted line); H3=late Pliocene discontinuity (~3.5-3.0 Ma; light blue dotted line); H4=early Quaternary discontinuity (~2.5-2.1 Ma; green dotted line); H5=mid Pleistocene discontinuity (~0.9-0.7 Ma; orange dotted line); H6=late Quaternary discontinuity (~0.47 Ma; red dotted line).

Fig. 9. Three-channel airgun seismic profile and the interpretation, showing 6 units (U1-U6) from the bottom to the top. Seismic terminations are indicated by red arrows. The location of this seismic line is displayed in Fig. 2a. H1= the Miocene base (black dotted line); H2=the Miocene top (~5.33 Ma; dark blue dotted line); H3=late Pliocene discontinuity (~3.5-3.0 Ma; light blue dotted line); H4=early Quaternary discontinuity (~2.5-2.1 Ma; green dotted line); H5=mid Pleistocene discontinuity (~0.9-0.7 Ma; orange dotted line); H6=late Quaternary discontinuity (~0.47 Ma; red dotted line).

Fig. 10. Isochore maps of units 1 to 6. The thicknesses are displayed in ms TWT (two-way travel time). Morpho-sedimentary interpretation on sedimentary deposition and associated processes are included.

Fig. 11. Sketch of the Pliocene-Quaternary evolution of the Le Danois CDS, including four stages: a) Onset (~5.3 to 3.5-3.0 Ma); b) Initial stage (3.5-3.0 to 2.5-2.1 Ma); c) Intermediate stage (2.5-2.1 to 0.9-0.7 Ma); d) Drift growth stage (0.9-0.7 Ma to present day).

Table 1. Description and examples of seismic facies of seismic stratigraphic units.

Table 1. Description and examples of seismic facies of seismic stratigraphic units.

Seismic stratigraphic units	Examples	Seismic facies
Unit 6 H6 to seafloor	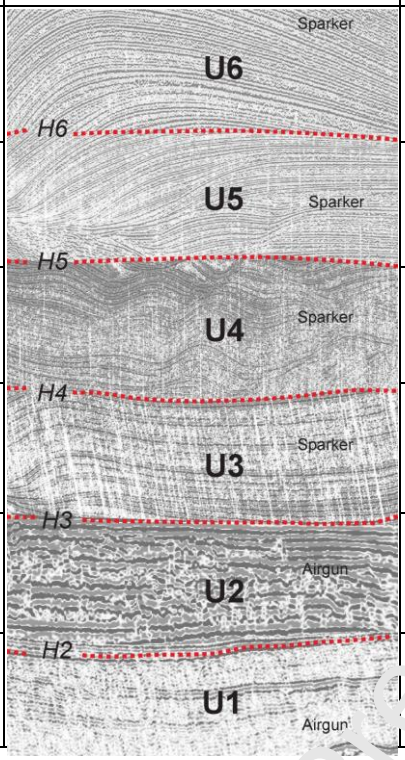	moderate-high amplitude, continuous oblique to subparallel reflections; mounded features are observed
Unit 5 H5 to H6		moderate-high amplitude, continuous oblique to subparallel reflections; mounded features with an upslope progradation are shown
Unit 4 H4 to H5		moderate-high amplitude, continuous oblique to subparallel reflections; wavy features are displayed at the central part of the bank
Unit 3 H3 to H4		moderate-high amplitude subparallel reflections; mounded features are shown along the southern foot of the bank
Unit 2 H2 to H3		high amplitude, disrupted/semi-continuous chaotic to subparallel reflections
Unit 1 H1 to H2		low-moderate amplitude, semi-continuous transparent to subparallel reflections

Highlights

- The MOW/AMW dominated SW European margins from the late Pliocene onwards.
- The Le Danois Drift was generated in both interglacial and glacial periods.
- Cyclic features of the Le Danois Drift lost their expression after the late Quaternary.
- Modern water masses may not be involved in the built-up of contourite drifts.